Available online at www.sciencedirect.com
SCIENCE DIRECT®
Electrochimica Acta 50 (2005) 1957–1964
ELECTROCHIMICA Acta
www.elsevier.com/locate/electacta

Effect of La/Ce ratio on the structure and electrochemical characteristics of $La_{0.7-x}Ce_xMg_{0.3}Ni_{2.8}Co_{0.5}$ ($x = 0.1$–0.5) hydrogen storage alloys

X.B. Zhang[a], D.Z. Sun[b], W.Y. Yin[a], Y.J. Chai[a], M.S. Zhao[a,*]

[a] *Key Laboratory of Rare Earth Chemistry and Physics, Changchun Institute of Applied Chemistry, Graduate School of Chinese Academy of Sciences, Chinese Academy of Sciences, No. 5625, Changchun 130022, PR China*

[b] *State Key Laboratory of Electro-analytical Chemistry, Changchun Institute of Applied Chemistry, Graduate School of Chinese Academy of Sciences, Chinese Academy of Sciences, Changchun 130022, PR China*

Received 3 August 2004; received in revised form 2 September 2004; accepted 3 September 2004
Available online 28 October 2004

Abstract

The effect of La/Ce ratio on the structure and electrochemical characteristics of the $La_{0.7-x}Ce_xMg_{0.3}Ni_{2.8}Co_{0.5}$ ($x = 0.1$, 0.2, 0.3, 0.4, 0.5) alloys has been studied systematically. The result of the Rietveld analyses shows that, except for small amount of impurity phases including LaNi and $LaNi_2$, all these alloys mainly consist of two phases: the $La(La, Mg)_2Ni_9$ phase with the rhombohedral $PuNi_3$-type structure and the $LaNi_5$ phase with the hexagonal $CaCu_5$-type structure. The abundance of the $La(La, Mg)_2Ni_9$ phase decreases with increasing cerium content whereas the $LaNi_5$ phase increases with increasing Ce content, moreover, both the *a* and cell volumes of the two phases decrease with the increase of Ce content. The maximum discharge capacity decreases from 367.5 mAh g^{-1} ($x = 0.1$) to 68.3 mAh g^{-1} ($x = 0.5$) but the cycling life gradually improve. As the discharge current density is 1200 mA g^{-1}, the HRD increases from 55.4% ($x = 0.1$) to 67.5% ($x = 0.3$) and then decreases to 52.1% ($x = 0.5$). The cell volume reduction with increasing *x* is detrimental to hydrogen diffusion *D* and accordingly decreases the low temperature dischargeability of the $La_{0.7-x}Ce_xMg_{0.3}Ni_{2.8}Co_{0.5}$ ($x = 0.1$–0.5) alloy electrodes.

Keywords: Structure characteristics; High rate dischargeability; Low temperature dischargeability; Exchange current density; Hydrogen diffusion coefficient

1. Introduction

According to the problem induced by the shortage of fossil energy and global warming, hydrogen is expected to be a promising energy vector for near future. In order for hydrogen to become a viable solution to the energy crisis and the environmental problems, storage processes must be improved in terms of specific capacity and security. Among different ways to store hydrogen, absorption in solid is very attractive since it allows safe storage at pressure and temperature close to ambient conditions [1]. There are many kinds of metals and alloys which are able to absorb large amount of hydrogen and they are used in many fields, such as heat pump, thermal storage system, as catalysts, fuel cells, nickel–metal hydride (Ni–MH) rechargeable batteries and so on.

In recent years, Ni–MH secondary batteries, in which hydrogen storage alloy is employed as negative electrode, have been widely adopted in various portable electronic devices, electric hand tools and electric vehicles because of their high reversible energy storage density, fast electrochemical activation, long cyclic stability, good charge/discharge kinetics and environmental compatibility [2–7]. To date, almost all commercial Ni–MH batteries are employing AB_5-type alloys as negative electrode materials because of their good overall electrode properties [8]. However, the electrochemical capacity of the AB_5-type alloys is limited by the single $CaCu_5$-type hexagonal structure [9], the energy densities of the Ni–MH batteries are not competing favorably with some other advanced secondary batteries. Therefore, new type alloys with higher energy density, faster activation, better rate

* Corresponding author. Tel.: +86 431 5262365; fax: +86 431 5685653.
E-mail address: zhaoms@ciac.jl.cn (M.S. Zhao).

0013-4686/$ – see front matter © 2004 Elsevier Ltd. All rights reserved.
doi:10.1016/j.electacta.2004.09.016

dischargeability and lower cost are urgently needed to replace the conventional rare earth-based AB_5-type alloys [10].

Recently, Kadir et al. [11–13] have reported the discovery of a new type of ternary alloys with the general formula of RMg_2Ni_9 (R: rare earth, Ca, Y) with $PuNi_3$ type structure. It is found that some of the R–Mg–Ni-based ternary alloys can absorb/desorb 1.8–1.87 wt.% H_2 and are thus regarded as promising candidates for reversible gaseous hydrogen storage [14,15]. As to their electrochemical hydrogen storage, Chen et al. [7] have studied the structure and electrochemical characteristics of $LaCaMg(Ni, M)_9$ (M = Al, Mn) alloys, and almost at the same time, Kohno et al. [16] have reported that the discharge capacity of $La_{0.7}Mg_{0.3}Ni_{2.8}Co_{0.5}$ alloy reached 410 mAh g^{-1}. However, up to now, the La–Mg–Ni–Co system hydrogen storage electrode alloys can not used as negative material of the Ni–MH secondary batteries due to theirs serious corrosion in KOH electrolyte [17]. Adzic et al. [18] pointed out that the rate of loss of electrochemical capacity per charge/discharge cycle due to electrode corrosion was significantly decreased due to the presence of Ce. Sakai et al. [19] reported that the replacement of lanthanum by large amounts of cerium gave the alloy a satisfactory cycle lifetime even in the low content range of cobalt.

In this work, on the basis of our previous studies and the belief that the Ce addition may result in some noticeable modification, the structure and electrochemical characteristics of the $La_{0.7-x}Ce_xMg_{0.3}Ni_{2.8}Co_{0.5}$ (x = 0.1–0.5) alloys has been investigated systematically.

2. Experimental details

2.1. Alloy preparation and X-ray diffraction analysis

All alloy samples were prepared by arc-melting carefully the constituent elements or master alloy on a water-cooled copper hearth under argon atmosphere. The purity of the metals, i.e., La, Ce, Mg, Ni and Co is higher than 99.9 mass%. The samples were all inverted and remelted 5 times to ensure good homogeneity. Thereafter, these alloy samples were mechanically crushed into fine powders of 300 mesh in mortar.

Crystallographic characteristics of the hydrogen storage alloys were investigated by X-ray diffraction on Rigaku D/Max 2500PC X-ray diffractometer (Cu Kα, monochromator) using JADE5 software [20].

2.2. Electrochemical measurement

The well-mixed alloy powder and carbonyl nickel powder in weight ratio of 1:5 were pressed into the tablets as metal hydride electrode, which had the diameter of 13 mm and thickness of 1.5 mm, and the weight of each electrode was about 0.9 g.

The electrochemical properties were then measured in a standard three electrode cell consisting of a working electrode (metal–hydride electrode), a counter-electrode ($NiOOH/Ni(OH)_2$ electrode) and a reference electrode (Hg/HgO electrode). The electrolyte in the cell was 6 M KOH aqueous solution. Charge and discharge tests were carried out on an automatic galvanostatic system (DC-5). The emphasis of these charge/discharge tests was on the electrochemical capacity and stability of the negative electrode, thus the capacity of the positive electrode plate was designed to be much higher than that of the negative electrode. At 298 K, these experimental cells were firstly charged at current of 60 mA g^{-1} for 7 h followed a rest for 30 min and were discharged at the same discharge current density to the cut-off voltage of −0.60 V versus Hg/HgO.

Pressure–composition isotherms (P–C–T) curves were electrochemically obtained by converting the equilibrium potential of the metal hydride electrode to the equilibrium pressure of hydrogen on the basis of Nernst equation using electrochemical data [21] as reported in reference [22]. The equilibrium potential curves were obtained by alternating the following two processes: (1) a pulse discharge of (25 mA g^{-1} × 0.25 h); and (2) a rest period until the potential became almost constant. The equilibrium potential change of approximately 30 mV corresponds to the equilibrium pressure change by one order of magnitude. Since the measured potentials have an error of 1–2 mV, the calculated pressure values are accurate to be within 10% [22].

To evaluate the high rate dischargeability (HRD) (in the range of 60–1200 mA g^{-1}), discharge capacities of the alloy electrode at different discharge current densities were measured. The high rate dischargeability (%) defined as $C_n \times 100/(C_n + C_{60})$, was determined from the ratio of the discharge capacity C_n (with n = 60, 240, 480, 720, 960, 1200 mA g^{-1}, respectively) to the total discharge capacity defined as the sum of C_n and C_{60} which was the additional capacity measured subsequently at 60 mA g^{-1} after C_n was measured.

For investigating the electrocatalytic activity of the hydrogen electrode reaction, the linear polarization curves of the electrode were plotted on an EG&G PARC's Model 273 Potentiostat/Galvanostat station by scanning the electrode potential at the rate of 0.1 mV $^{-s}$ from −5 to 5 mV (versus open circuit potential) at 50% depth of discharge (DOD) at 298 K. The polarization resistance R_p can be obtained from the slope of the linear polarization curves. Moreover, the exchange current density (I_0), which is a measure of the catalytic activity of electrode, was calculated from the slopes of polarization curves by the following equation [23],

$$I_0 = \frac{RT}{FR_p}$$

where R is the gas constant, T the absolute temperature, F the Faraday constant, and R_p the polarization resistance. The potentiostatic discharge technique was used to evaluate the coefficient of diffusion within the bulk of the alloy electrodes. After being fully charged followed by a 30 min open-circuit lay-aside, the test electrodes were discharged with +500 mV potential-step for 500 s on a EG&G PARC's

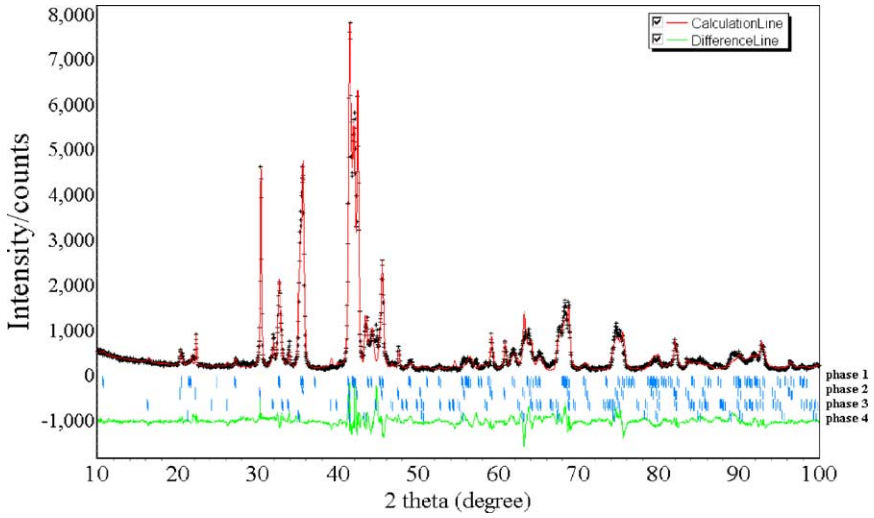

Fig. 1. Rietveld profiles refinement of XRD patterns $La_{0.6}Ce_{0.1}Mg_{0.3}Ni_{2.8}Co_{0.5}$ alloy (Phase 1: La(La, Mg)$_2$Ni$_9$; Phase 2: $LaNi_5$; Phase 3: LaNi; Phase 4: $LaNi_2$).

Model 273 Potentiostat/Galvanostat station, using the M352 CorrWare electrochemical/corrosion software.

3. Results and discussion

3.1. Structure characteristic

Fig. 1 shows the Rietveld analysis pattern of the $La_{0.6}Ce_{0.1}Mg_{0.3}Ni_{2.8}Co_{0.5}$ hydrogen storage alloy as an example of $La_{0.7-x}Ce_xMg_{0.3}Ni_{2.8}Co_{0.5}$ ($x = 0.1$–0.5) alloys. It can be found that, except for small amounts of impurity phase including LaNi and $LaNi_2$, the $La_{0.6}Ce_{0.1}Mg_{0.3}Ni_{2.8}Co_{0.5}$ alloy mainly consisted of a La_2MgNi_9 phase with a $PuNi_3$-type rhombohedral structure and a $LaNi_5$ phase with a $CaCu_5$-type hexagonal structure. Furthermore, it can be derived that the Mg atoms only occupy the 6c sites and the La atoms can occupy both the 3a and the 6c sites in the phase with rhombohedral (Space group: *R*-3*m* 166) $PuNi_3$-type structure by Rietveld refinement. So the final structure of La_2MgNi_9 phase can be designated as La(La, Mg)$_2$Ni$_9$. The lattice parameters, cell volume and phase abundance of $La_{0.7-x}Ce_xMg_{0.3}Ni_{2.8}Co_{0.5}$ ($x = 0.1$–0.5) alloys are all presented in Table 1. It can be seen that all the $La_{0.7-x}Ce_xMg_{0.3}Ni_{2.8}Co_{0.5}$ ($x = 0.1$–0.5) alloys are composed of the La(La, Mg)$_2$Ni$_9$ phase and $LaNi_5$ phase besides some minor impurity phases, $LaNi_2$ or LaNi. Moreover, we can find that cell volume of the La(La, Mg)$_2$Ni$_9$ phase and

Table 1
Characteristics of alloy phases in $La_{0.7-x}Ce_xMg_{0.3}Ni_{2.8}Co_{0.5}$ ($x = 0.1$–0.5) alloys

Samples	Phases	Phase abundance (wt.%)	Parameters of fit[a]	Lattice parameter (Å)			Cell volume (Å)
				a	*b*	*c*	
$x = 0.1$	La(La, Mg)$_2$Ni$_9$	76.54	$R_p = 10.1$, $R_{wp} = 13.8$	5.0672	5.0672	24.3851	542.24
	$LaNi_5$	21.21		5.0460	5.0460	3.9920	88.03
	LaNi	1.34		3.8761	10.7594	4.3234	180.31
	$LaNi_2$	0.91		7.2123	7.2123	7.2123	375.16
$x = 0.2$	La(La, Mg)$_2$Ni$_9$	69.78	$R_p = 8.7$, $R_{wp} = 11.4$	5.0425	5.0425	24.3247	535.64
	$LaNi_5$	27.68		5.0233	5.0233	4.0007	87.43
	LaNi	2.54		3.8343	10.7465	4.3229	178.13
$x = 0.3$	La(La, Mg)$_2$Ni$_9$	61.56	$R_p = 10$, $R_{wp} = 13.7$	5.0035	5.0035	24.2478	525.72
	$LaNi_5$	37.23		5.0004	5.0004	4.0028	86.68
	LaNi	1.21		3.8240	10.7321	4.2981	176.39
$x = 0.4$	La(La, Mg)$_2$Ni$_9$	58.68	$R_p = 5.7$, $R_{wp} = 7.8$	4.9691	4.9691	24.1138	515.65
	$LaNi_5$	39.35		4.9728	4.9728	4.0064	85.8
	LaNi	1.97		3.7860	10.7258	4.2696	173.38
$x = 0.5$	La(La, Mg)$_2$Ni$_9$	53.65	$R_p = 8.6$, $R_{wp} = 11.2$	4.9372	4.9372	23.9985	506.61
	$LaNi_5$	43.23		4.9512	4.9512	4.0097	85.13
	LaNi	3.12		3.6762	10.7023	4.2506	167.23

The Rietveld refinement program RIETICA was used.
[a] R_p: the pattern factor; R_{wp}: the weighted pattern factor.

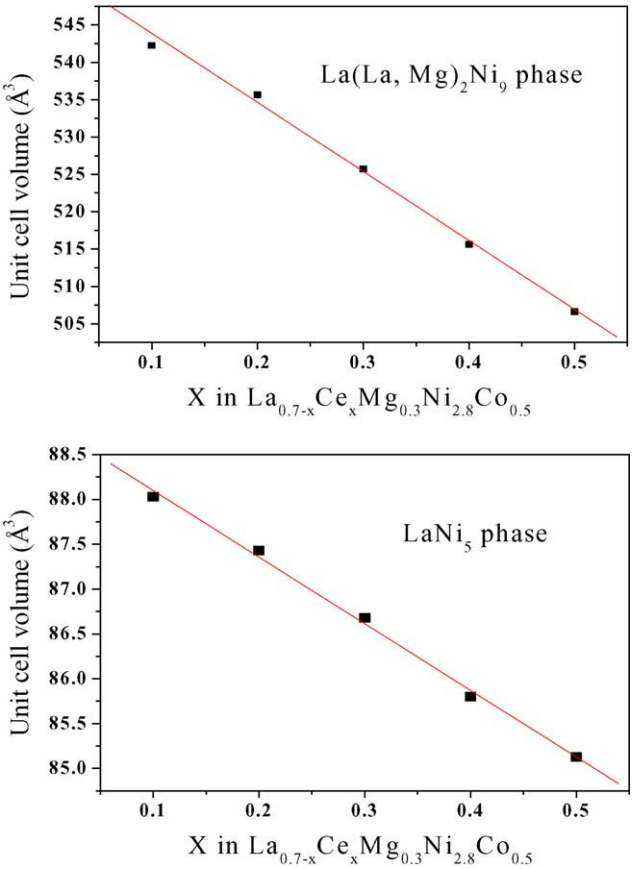

Fig. 2. Variation of the unit cell volume of the La(La, Mg)$_2$Ni$_9$ and LaNi$_5$ with x.

the LaNi$_5$ phase in the alloys all decrease monotonically with the increase of x, which can be attributed to the fact that the atomic radius of Ce (1.824 Å) is smaller than that of La (1.877 Å). The unit cell volume of the La(La, Mg)$_2$Ni$_9$ and LaNi$_5$ as a function of x in $La_{0.7-x}Ce_xMg_{0.3}Ni_{2.8}Co_{0.5}$ ($x = 0.1$–0.5) alloys is shown in Fig. 2. The cell volume is of interest because it can be correlated with the stability of the hydride phase in any homologous alloys series [21]. The cell volume is also a linear function of the Ce content and a useful check on the intermetallic composition [22]. The equation for the cell volume of La(La, Mg)$_2$Ni$_9$ phase as a function of x is:

$$\text{cell volume} = (553.959 - 92.39x)\,\mathring{A}^3 \quad (1)$$

and the relationship between the cell volume of LaNi$_5$ phase and x can be expressed as:

$$\text{cell volume} = (88.843 - 7.43x)\,\mathring{A}^3 \quad (2)$$

The Fig. 3 shows the abundances of the La(La, Mg)$_2$Ni$_9$ phase and the LaNi$_5$ phase as a function of x in the $La_{0.7-x}Ce_xMg_{0.3}Ni_{2.8}Co_{0.5}$ ($x = 0.1$–0.5) alloys. As can be seen in Fig. 3 and Table 1, the La(La, Mg)$_2$Ni$_9$ phase abundance decreases from 76.54% to 53.65% with increasing x, however, the LaNi$_5$ phase abundance increases from 21.2% to 43.23%. These results may influence the hydrogen storage and electrochemical characteristics of the alloys studied.

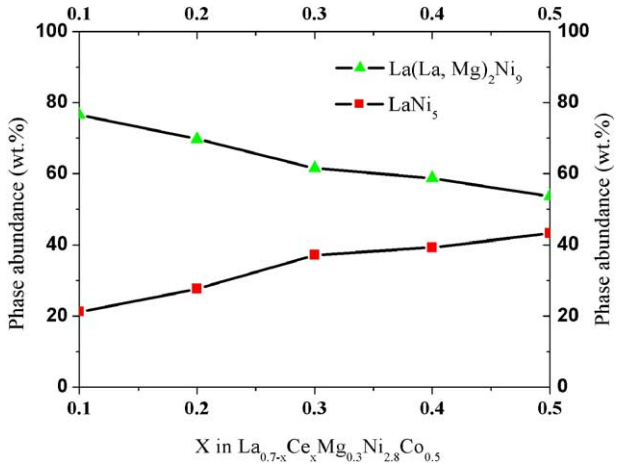

Fig. 3. Phase abundance of the La(La, Mg)$_2$Ni$_9$ phase and the LaNi$_5$ phase existing in the $La_{0.7-x}Ce_xMg_{0.3}Ni_{2.8}Co_{0.5}$ ($x = 0.1$–0.5) alloys.

3.2. P–C isotherms

The electrochemical pressure–composition isotherms method is very useful for examining the charging and discharging levels of hydrogen in an anode, although the calculated pressures pertain to a quasi-equilibrium state [23]. The P–C–T curves for hydrogen desorption in the $La_{0.7-x}Ce_xMg_{0.3}Ni_{2.8}Co_{0.5}$-H system at 298 K are presented in Fig. 4.

With the increase of x, the plateau pressure of the $La_{0.7-x}Ce_xMg_{0.3}Ni_{2.8}Co_{0.5}$ ($x = 0.1$–0.5) alloys increases monotonously and the plateau region becomes narrower and steeper, which leads to the decrease of the hydrogen storage capacity (H/M) from 0.952 to 0.177. This result is in good agreement with that reported by Liu et al. [22]. The change of the P–C–T characteristics can be mainly attributed to the reduction of the unit cell volume and the relative change of phase abundance of La(La, Mg)$_2$Ni$_9$ phase and LaNi$_5$ phase. The increase of the plateau pressure of the $La_{0.7-x}Ce_xMg_{0.3}Ni_{2.8}Co_{0.5}$ hydrogen storage alloy can

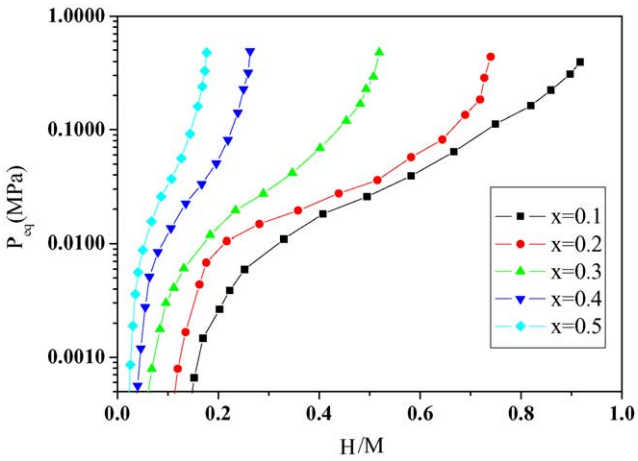

Fig. 4. The electrochemical desorption P–C–T curves for $La_{0.7-x}Ce_x$ $Mg_{0.3}Ni_{2.8}Co_{0.5}$ ($x = 0.1$–0.5) alloy electrodes at 298 K.

be mainly ascribed to two reasons. On the one hand, it is well known that unit cell of the AB_3 compounds contains one-third AB_5 and two-third AB_2 structure [7,10] and thus the plateau pressure of the La(La, Mg)$_2$Ni$_9$ phase is similar to that of $LaNi_5$ phase. In fact, the plateau of the La(La, Mg)$_2$Ni$_9$ phase is slightly lower than that of the $LaNi_5$ phase. With the increase of Ce content, as mentioned above, the abundance of La(La, Mg)$_2$Ni$_9$ phase decreases whereas the phase abundance of the $LaNi_5$ phase increases, which thereby slightly increases the plateau pressure of the $La_{0.7-x}Ce_xMg_{0.3}Ni_{2.8}Co_{0.5}$ hydrogen storage alloy. On the other hand, the cell volume of both the La(La, Mg)$_2$Ni$_9$ phase and the $LaNi_5$ phase decreases with increasing Ce content, as shown in Table 1 and Fig. 2, which will also inevitably increases the plateau pressure of the $La_{0.7-x}Ce_xMg_{0.3}Ni_{2.8}Co_{0.5}$ hydrogen storage alloy. Precheron-Guegan et al. [24] pointed out that the hydrogen absorbed in a hydrogen storage alloy enters and stays in the atomic state in the interstitial cavities of crystal lattice of the alloy. So the crystal structure of the alloy plays an important role on the hydrogen storage performance, especially the hydrogen storage capacity. Alloys with bigger cell volumes and hence bigger interstitial cavities generally have larger hydrogen storage capacity. The cell volumes of both La(La, Mg)$_2$Ni$_9$ phase and $LaNi_5$ phase decrease with the increase of the Ce content, which inevitably lowers the hydrogen storage capacity. Those lends credence to our assumption that the change of hydrogen storage capacity for $La_{0.7-x}Ce_xMg_{0.3}Ni_{2.8}Co_{0.5}$ alloys results from the relative variation of the phase abundance of the La(La, Mg)$_2$Ni$_9$ phase and $LaNi_5$ phase.

3.3. Activation, maximum discharge capacity and cycle stability

Fig. 5 shows the activation profiles of the $La_{0.7-x}Ce_xMg_{0.3}Ni_{2.8}Co_{0.5}$ ($x = 0.1$–0.5) alloy electrodes. Both the first cycle and the maximum discharge capacity decrease with the increases of the Ce content. It can be seen that

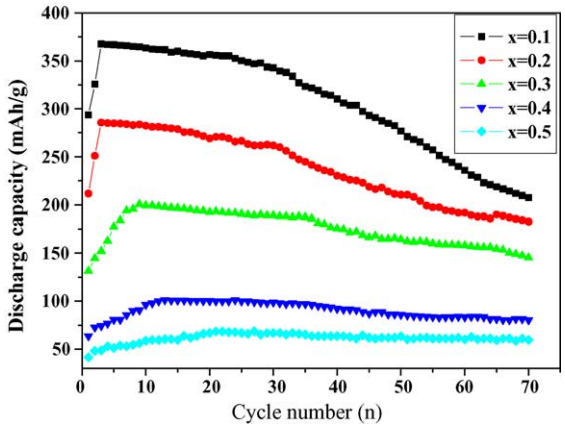

Fig. 5. The cycle life curves of the $La_{0.7-x}Ce_xMg_{0.3}Ni_{2.8}Co_{0.5}$ ($x = 0.1$, 0.2, 0.3, 0.4, 0.5) alloy electrodes at 298 K.

Table 2
Summary of the electrode performance of $La_{0.7-x}Ce_xMg_{0.3}Ni_{2.8}Co_{0.5}$ ($x = 0.1$–0.5) alloy electrodes

Samples	H/M	C_{max} (mAh g^{-1})	N_a[a]	HRD$_{1200}$ (%)[b]	S_{70} (%)
$x = 0.1$	0.952	367.5	3	55.4	56.4
$x = 0.2$	0.740	285.7	3	60.3	63.9
$x = 0.3$	0.519	200.4	9	67.5	72.5
$x = 0.4$	0.263	101.3	13	58.1	79.3
$x = 0.5$	0.177	68.3	21	52.1	87.3

[a] Cycle numbers needed to activate the electrodes.
[b] High rate dischargeability at a discharge current density of 1200 mA g^{-1}.

their activations become slower with an increase of Ce content, which is in good agreement with the results reported by Adzic et al. [25]. The cycles needed to activate the electrodes and the maximum discharge capacities of the alloy electrodes are summarized in Table 2. With the increase of x, the maximum discharge capacity of the alloy electrode decreases from 367.5 mAh g^{-1} ($x = 0.1$) to 68.3 mAh g^{-1} ($x = 0.5$)*a*, which is in good agreement with the results of P–C–T curves measurement. The cycling capacity retention rate, expressed as $S_{70}(\%) = C_{70}/C_{max} \times 100$ (where C_{max} is the maximum discharge capacity, C_{70} is the discharge capacity at the 70th cycle), after 70 cycles at 60 mA g^{-1} is also listed in Table 2. As seen in Fig. 5 and Table 2, it is found that the capacity retention rate (S_{70}) improves gradually with increasing Ce content. There are two major effects of La/Ce ratio on the electrochemical cycling stability of $La_{0.7-x}Ce_xMg_{0.3}Ni_{2.8}Co_{0.5}$ ($x = 0.1-0.5$) alloy electrodes. First is the effect of the unit-cell volume which decreases with increasing cerium contents. It is generally believed that the volume change of an alloy during hydriding is proportional to the amount of hydrogen absorbed in alloy or to the electrochemical capacity. The increase of the Ce content generally leads to a smaller lattice cavity and lower hydrogen storage capacity and smaller changer of unit cell on hydriding and hence less pulverization and improvement in the cycling life. The second is the formation of a protective surface film. As the Ce^{3+} ions can be oxidized to Ce^{4+} ions in the alkaline electrolyte they form a dense and strong CeO_2 oxide film on the alloy surface. The dense oxide film rather effectively inhibits further oxidation of the alloy and slows down the corrosion rate and thereby, improves the cyclic stability of the alloy.

3.4. High rate dischargeability

Fig. 6 shows the effect of the discharge current density (60–1200 mA g^{-1}) on the discharge capacity of the $La_{0.7-x}Ce_xMg_{0.3}Ni_{2.8}Co_{0.5}$ ($x = 0.1$–0.5) alloy electrodes. The HRD of the alloy electrodes for the discharge current density of 1200 mA g^{-1} are also listed in Table 2. It can be seen that as x increases, the HRD of the alloy electrodes increases first and then decreases. Taking the discharge current density being 1200 mA g^{-1} as an example, the HRD of the alloy electrodes increases from 55.4% ($x = 0.1$) to 67.5% ($x = 0.3$) and then decreases to 52.1% ($x = 0.5$). This is an indication of the

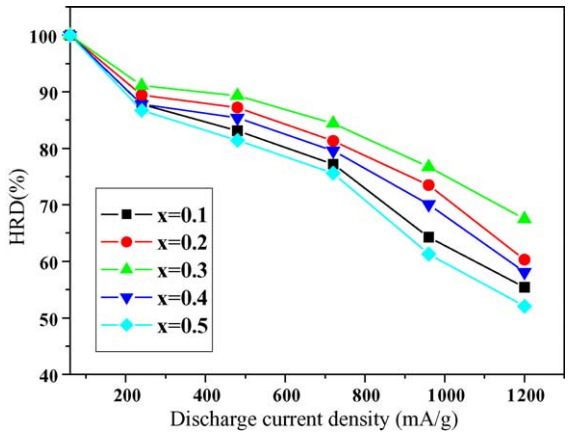

Fig. 6. The high rate dischargeability (HRD) of the $La_{0.7-x}Ce_xMg_{0.3}Ni_{2.8}Co_{0.5}$ ($x = 0.1$, 0.2, 0.3, 0.4, 0.5) alloy electrodes at 298 K.

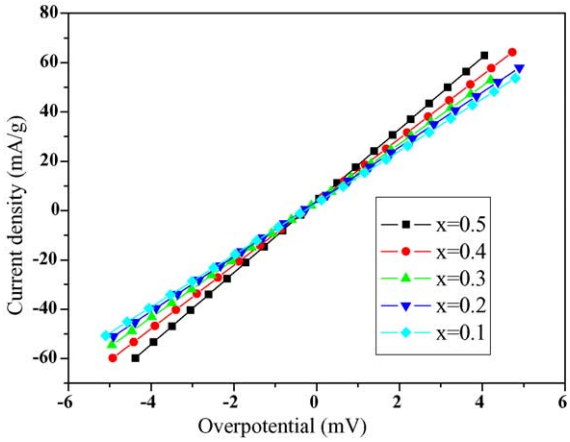

Fig. 7. Linear polarization curves for the $La_{0.7-x}Ce_xMg_{0.3}Ni_{2.8}Co_{0.5}$ ($x = 0.1$–0.5) alloy electrodes at the 50% depth of discharge (DOD) and 298 K.

occurrence of two opposing factors that contribute to the HRD of the alloy electrodes. It is generally accepted that the high rate dischargeability of a metal–hydride electrode is mainly determined by the charge-transfer process occurring at the metal electrolyte interface and the hydrogen diffusion process in the hydride bulk [26,27]. Fig. 7 shows the linear polarization curves of the $La_{0.7-x}Ce_xMg_{0.3}Ni_{2.8}Co_{0.5}$ ($x = 0.1$–0.5) alloy electrodes at 50% DOD and at 298 K. The polarization resistance R_p and exchange current density I_0 of the alloy electrodes are obtained and listed in Table 3. It can be seen that the polarization resistance R_p of the alloy electrodes decreases from 94.8 mΩ ($x = 0.1$) to 68.7 mΩ ($x = 0.5$), accordingly the exchange current density I_0 of the alloy electrodes increases from 270.9 to 373.6 mA g^{-1} when x increases from 0.1 to 0.5. Pan [28] pointed that, for La–Mg–Ni–Co system alloys, the $LaNi_5$ phase works not only as a hydrogen reservoir, but also as a catalyst to activate the $La(La, Mg)_2Ni_9$ phase to absorb/desorb hydrogen reversibly in the alkaline electrolyte [24]. The $LaNi_5$ phase abundance increases with increasing Ce content, as mentioned above and hence increases the exchange current density I_0 of the alloy electrodes. The diffusion coefficient of hydrogen in the bulk of the alloys was determined by means of the potential-step method and also listed in Table 3. The hydrogen diffusion coefficient decreases from 15.17×10^{-10} $cm^{2\ -s}$ ($x = 0.1$) to 7.32×10^{-10} $cm^{2\ -s}$ ($x = 0.5$), which can be attributed to the reduction of cell volume of the alloys with increasing Ce content. With the increase of x in $La_{0.7-x}Ce_xMg_{0.3}Ni_{2.8}Co_{0.5}$ ($x = 0.1$–0.5) alloy electrodes, the exchange current density I_0 increase monotony, whereas the hydrogen diffusion coefficient D decrease linearly. Overall, the combined effect of the two opposing factors will thereby result in an optimal value of x for HRD. The optimal value of Ce content for $La_{0.7-x}Ce_xMg_{0.3}Ni_{2.8}Co_{0.5}$ ($x = 0.1$–0.5) system hydrogen alloy is 0.3 from our work.

3.5. Low temperature dischargeability (LTD)

It has been reported that the discharge capacity of the negative electrode in nickel–metal hydride decrease drastically with decreasing temperature [29]. Sakai et al. [30] pointed out that the dischargeability of the negative electrodes at relative low temperature depended on the hydrogen diffusion and/or charge-transfer process occurring at the metal–electrolyte interface. The hydrogen diffusion coefficient (D) of hydrogen in the bulk is evaluated using the method described by Iwakura et al. [31]. The LTD, expressed as $LTD_{233}(\%) = C_{233}/C_{298} \times 100$ (where C_{233} and C_{298} are the discharge capacity at 233 K and 298 K, respectively). The hydrogen diffusion coefficient (D) and the exchange current density (I_0) of the $La_{0.7-x}Ce_xMg_{0.3}Ni_{2.8}Co_{0.5}$ ($x = 0.1$–0.5) alloy electrodes at 233 K are also listed in Table 3. It can found that both the I_0 and the D are smaller than that at

Table 3
Electrochemical kinetic parameters of $La_{0.7-x}Ce_xMg_{0.3}Ni_{2.8}Co_{0.5}$ ($x = 0.1$–0.5) alloy electrodes.

Samples	Polarization resistance, R_p (mΩ)		Exchange current density, I_0 (mA g^{-1})		Hydrogen diffusion coefficient (D) ($\times 10^{-10}$ $cm^{2\ -s}$)	
	298 K	233 K	298 K	233 K	298 K	233 K
$x = 0.1$	94.8	872	270.9	23.0	15.17	3.53
$x = 0.2$	90.1	863	285.1	23.3	14.32	2.78
$x = 0.3$	85.1	859	301.7	23.4	13.14	2.16
$x = 0.4$	77.8	852	330.1	23.6	9.34	1.73
$x = 0.5$	68.7	849	373.6	23.6	7.32	0.97

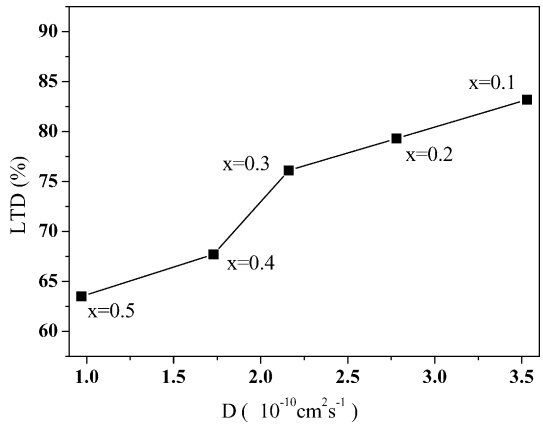

Fig. 8. The low temperature dischargeability (LTD) as a function of hydrogen diffusion coefficient (D) of the $La_{0.7-x}Ce_xMg_{0.3}Ni_{2.8}Co_{0.5}$ ($x = 0.1$, 0.2, 0.3, 0.4, 0.5) alloy electrodes at 233 K.

298 K. Moreover, we can find that the I_0 maintain almost unchanged (23.0–23.6 mA g^{-1}) and, whereas D decreases remarkably with increasing x, which implies that the hydrogen diffusion in alloy probably becomes the rate-determining factor for low temperature dischargeability at 233 K. Fig. 8 shows LTD as a function of D in $La_{0.7-x}Ce_xMg_{0.3}Ni_{2.8}Co_{0.5}$ ($x = 0.1$–0.5) alloy electrodes. It can be easily found that D decreases with the increase of x, which can be attributed to the cell volume reduction with increasing x as shown in Table 1. The decreasing D accordingly decreases the LTD of $La_{0.7-x}Ce_xMg_{0.3}Ni_{2.8}Co_{0.5}$ ($x = 0.1$–0.5) alloy electrodes.

4. Conclusion

In this paper, the effect of the cerium content on the structural and electrochemical characteristics of the $La_{0.7-x}Ce_xMg_{0.3}Ni_{2.8}Co_{0.5}$ ($x = 0.1$–0.5) hydrogen storage alloys has been studied systematically. It is found by XRD Rietveld analysis that, except for small amount of impurity phases including LaNi and $LaNi_2$, all these alloys mainly consist of two phases: the La(La, $Mg)_2Ni_9$ phase with the rhombohedral $PuNi_3$-type structure and the $LaNi_5$ phase with the hexagonal $CaCu_5$-type structure. The abundance of the La(La, $Mg)_2Ni_9$ phase decreases with increasing cerium content, whereas the $LaNi_5$ phase increases with increasing Ce content. The P–C isotherm curves show that with increasing Ce content in the alloys, the plateau pressure of the hydrogen desorption increases steeply and the plateau region becomes narrower and steeper. It is found that with increasing Ce content the discharge capacity decreases and the cycling life can be gradually improved. The high rate dischargeability (HRD) and the exchange current density I_0 of the alloy electrodes increases from $x = 0.1$ to 0.3 and then decreases with further increase of Ce content. The hydrogen diffusion coefficient D decreases with the increases of Ce content and thus decreases the low temperature dischargeability of $La_{0.7-x}Ce_xMg_{0.3}Ni_{2.8}Co_{0.5}$ ($x = 0.1$–0.5) alloy electrodes.

Acknowledgement

This work was financially supported by the National Natural Science Foundation of China (Grant No. 20171042).

References

[1] M. Latroche, A. Percheron-Guegan, J. Alloys Comp. 356–357 (2003) 461.
[2] J.J.G. Willems, K.H.J. Buschow, J. Less-Common Met. 129 (1987) 13.
[3] T. Sakai, H. Miyamura, N. Kuriyama, A. Kato, K. Oguro, H. Ishikawa, J. Electrochem. Soc. 137 (1990) 795.
[4] T. Kohno, H. Yoshida, F. Kawashima, T. Inaba, I. Sakai, M. Yamamoto, M. Kanda, J. Alloys Comp. 311 (2000) L5.
[5] J.J.G. Willems, Philips J. Res. 39 (Suppl. 1) (1984) 1.
[6] H.G. Pan, Y.F. Zhu, M.X. Gao, Q.D. Wang, J. Electrochem. Soc. 149 (2002) 829.
[7] J. Chen, N. Kuriyama, H.T. Takeshita, H. Tanaka, T. Sakai, M. Haruta, Electrochem. Solid-State Lett. 3 (6) (2000) 249.
[8] T. Sakai, I. Uehara, H. Iwakura, J. Alloys Comp. 293–295 (1999) 762.
[9] J.J. Reilly, G.D. Adzic, J.R. Johnson, T. Vogt, S. Mukerjee, J. McBreen, J. Alloys Comp. 293–295 (1999) 569.
[10] Y.F. Liu, H.G. Pan, Y.F. Zhu, R. Li, Y.Q. Lei, Mater. Sci. Eng. A. A372 (2004) 163.
[11] K. Kadir, T. Sakai, I. Uahara, J. Alloys Comp. 257 (1997) 115.
[12] K. Kadir, N. Nuriyama, T. Sakai, I. Uehara, L. Eriksson, J. Alloys Comp. 284 (1999) 145.
[13] K. Kadir, T. Sakai, I. Uahara, J. Alloys Comp. 287 (1999) 264.
[14] K. Kadir, T. Sakai, I. Uahara, J. Alloys Comp. 302 (2000) 112.
[15] J. Chen, H.T. Takeshita, H. Tanaka, N. Kuriyama, T. Sakai, J. Alloys Comp. 302 (2000) 304.
[16] T. Kohno, H. Yoshida, F. Kawashima, T. Inaba, I. Sakai, M. Yamamoto, M. Kanda, J. Alloys Comp. 311 (2000) 5.
[17] B. Liao, Y.Q. Lei, L.X. Chen, G.L. Lu, H.G. Pan, Q.D. Wang, J. Power Sources 129 (2004) 358.
[18] G. Adzic, J.R. Johnson, J.J. Reilly, J. McBreen, S. Mukerjee, M.P.S. Kumar, W. Zhang, S. Srinivasan, J. Electrochem. Soc. 142 (1995) 3429.
[19] T. Sakai, T. Hazama, H. Miyamura, N. Kuriyama, A. Kato, H. Ishikawa, J. Less-Common Met. 172–174 (1991) 1175.
[20] Materials Data JADE Release 5, XRD pattern processing, Materials Data Inc. (MDI), 1997.
[21] D.N. Gruen, M.H. Mendelsohn, A.E. Dwight, J. Less-Common Met. 161 (1977) 193.
[22] H.G. Pan, Q.W. Jin, M.X. Gao, Y.F. Liu, R. Li, Y.Q. Lei, J. Alloys Comp. 373 (2004) 237.
[23] T. Sakai, H. Miyamura, N. Kuriyama, A. Kato, K. Oguro, H. Ishikawa, J. Less-Common Met. 159 (1990) 127.
[24] A. Precheron-Guegan, C. Lartigue, J.C. Achard, J. Less-Common Met. 161 (1990) 193.
[25] G.D. Adzic, J.R. Johnson, J.J. Reilly, J. McBreen, S. Mukerjee, M.P. Sridhar Kumar, W. Zhang, S. Srinivasan, J. Electrochem. Soc. 142 (1995) 3429.

[26] C. Iwakura, T. Oura, H. Inoue, M. Matsuoka, Electrochem. Acta 41 (1) (1996) 117.
[27] C. Iwakura, M. Matsuoka, K. Asai, T. Kohno, J. Power Source 38 (1992) 335.
[28] H.G. Pan, Y.F. Liu, M.X. Gao, Y.Q. Lei, Q.D. Wang, J. Electrochem. Soc. 150 (5) (2003) 565.
[29] H. Senoh, Y. Hara, H. Inoue, C. Iwakura, Electrochim. Acta 46 (2001) 967.
[30] T. Sakai, H. Miyamura, N. Kuriyama, A. Kato, K. Ogura, H. Ishikawa, J. Electrochem. Soc. 137 (1990) 795.
[31] C. Iwakura, H. Senoh, K. Morimoto, Y. Hara, H. Inoue, Electrochemistry 70 (1) (2002) 2.